Pump-controlled modal interactions in microdisk lasers

Seng Fatt Liew,[1] Li Ge,[2,3] Brandon Redding,[1] Glenn S. Solomon,[4] and Hui Cao[1,*]
[1]*Department of Applied Physics, Yale University, New Haven, Connecticut 06520, USA*
[2]*Department of Engineering Science and Physics, College of Staten Island, CUNY, Staten Island, New York 10314, USA*
[3]*The Graduate Center, CUNY, New York, New York 10016, USA*
[4]*Joint Quantum Institute, NIST and University of Maryland, Gaithersburg, Maryland 20899, USA*
(Received 29 December 2014; published 20 April 2015)

We demonstrate an effective control of nonlinear interactions of lasing modes in a semiconductor microdisk cavity by shaping the pump profile. A target mode is selected at the expense of its competing modes either by increasing their lasing thresholds or suppressing their power slopes above the lasing threshold. Despite the strong spatial overlap of the lasing modes at the disk boundary, adaptive pumping enables an efficient selection of any lasing mode to be the dominant one, leading to a switch of lasing frequency. The theoretical analysis illustrates both linear and nonlinear effects of selective pumping and quantifies their contributions to lasing-mode selection. This work shows that adaptive pumping not only provides a powerful tool to control the nonlinear process in multimode lasers, but also enables the tuning of lasing characteristic after the lasers have been fabricated.

DOI: 10.1103/PhysRevA.91.043828 PACS number(s): 42.55.Sa, 42.60.Da, 42.25.Gy

I. INTRODUCTION

Multimode lasers are a classical example of nonlinear open systems that display complex behaviors. Recently, there has been growing interest and effort in understanding and manipulating the properties and interactions of lasing modes [1–7]. For example, the non-Hermitian physics of exceptional points has been explored for the control of lasing in coupled cavities [8–11]. The parity-time symmetry or, more specifically, the balanced gain and loss distribution in space has been utilized for lasing-mode selection [12–14]. These processes, however, only target the modification of the linear properties of individual lasing modes, including their respective thresholds and power. It would be fascinating, but more difficult, to manipulate their nonlinear interactions. Lately, active control of the pump profile for random lasers has been proposed and demonstrated using the spatial light modulator (SLM) [4,6,15,16], and it was found that nonuniform pumping enables a highly complex nonlinear modal interaction.

While these studies show it is possible to realize preferably single-mode, frequency-switchable, on-chip coherent light sources by controlling the pump profile, several fundamental questions must be addressed first, including (1) whether each of the lasing modes can be modified by the pump profile similar to that in random lasers, (2) if lasing modes are strongly overlapped in space, whether a desired mode can be selected via the pump control while the others are suppressed, and (3) how important the contributions from the linear effect (spatial overlap between the pump and the mode) and from the nonlinear effect (mode competition and gain saturation) are for lasing-mode selection.

In this work, we present a thorough experimental and theoretical study in the platform of the semiconductor microdisk laser, which has been utilized for single-photon emitters and biochemical sensors in integrated photonic circuits [17,18] and shown potential tunability as a pump-controlled device [19]. Such a feature is unexpected from the results of previous studies, which rely on the enhanced spatial overlap of the target mode with the pumping pattern or the pump-induced modification of the spatial mode profile for lasing-mode selection.

First, while the modes of a weakly scattering random laser can adapt themselves to the spatially inhomogeneous pumping pattern to facilitate lasing in the target mode, the lasing modes in a semiconductor microdisk are much more rigid, as they are tightly confined by total internal reflection at the disk boundary. Typically, the lasing modes correspond to the whispering-gallery (WG) modes with a low radial number, thanks to their high-quality (Q) factor and the resulting low lasing threshold. These modes are barely modified by the pump profile, as confirmed experimentally from their emission patterns [19]. Therefore, pump-controlled tunability cannot be achieved through the modification of each individual mode in a microdisk laser.

Second, the only possibility remaining for realizing a pump-controlled microdisk laser is then through the differentiation of individual lasing modes. Lasing in a selected mode may be facilitated by reducing its lasing threshold via increasing its spatial overlap with the pump profile [20–31]. To differentiate multiple lasing modes then requires little spatial overlap of this desired mode with all other modes; otherwise, lasing in nonselected modes would be enhanced as well. Unfortunately, the high-Q WG modes in a microdisk have very strong spatial overlap at the disk boundary, especially the ones with the same radial number, making mode selection almost impossible unless subwavelength control of the pump profile can be realized. This pessimistic outlook, however, applies only to a perfectly round microdisk. In practice, there is always inherent cavity surface roughness introduced unintentionally during the fabrication process. The coupling between high-Q WG modes of low radial numbers and lower-Q WG modes of higher radial numbers, caused by the surface roughness [32–34], enhances the spatial diversity of the lasing WG modes, which plays a critical role to differentiate the WG modes by adaptive pumping.

Experimentally, we find that selective pumping changes not only the lasing threshold but also the power slope of each WG mode in a semiconductor microdisk, which shows that

*hui.cao@yale.edu

both the linear and nonlinear effects caused by the spatially inhomogeneous pump profile are important. To suppress lasing in all nonselected modes, the threshold of the selected mode often increases too. The selected mode is not necessarily the first mode to lase (i.e., with the lowest lasing threshold); instead, it may grow the fastest and become the dominant lasing mode at high pumping level. Our theoretical analysis is able to differentiate the linear and nonlinear effects of selective pumping and quantify their contributions to lasing-mode selection.

Below we discuss these findings in detail, demonstrating that the adaptive pumping not only provides a powerful tool for controlling the nonlinear process in multimode lasers, but also enables the tuning of lasing characteristic after the lasers have been fabricated. We first present the experimental findings and then analyze them using the semiclassical laser theory.

II. ADAPTIVE PUMPING OF A MICRODISK LASER

The experiments were conducted on circular microdisks of larger radius and smaller boundary deformation than the ones used in Ref. [19]. The larger radius reduces the free spectral range and hence increases the number of possible lasing modes within the same gain bandwidth. Although many more modes managed to lase under uniform pumping, we were able to make every single one of them the dominant lasing mode with adaptive pumping. Interestingly, we observed different scenarios for the selected modes to win the competition, as described below.

A 200-nm-thick GaAs layer and a 1000-nm-thick $Al_{0.75}Ga_{0.25}As$ layer were grown on a GaAs substrate by molecular beam epitaxy. Three layers of InAs quantum dots were embedded in the middle of the GaAs layer. The circular disks of radius 10 μm were patterned by electron-beam lithography and followed by two steps of etching. The first is an inductively-coupled-plasma reactive etching with a BCl_3 and Cl_2 mixture to create $GaAs/Al_{0.75}Ga_{0.25}As$ cylinders. The second is a selective hydrofluoric acid based etching of the $Al_{0.75}Ga_{0.25}As$ to create a pedestal underneath the disk. Figure 1 shows the scanning electron microscope (SEM) images of a fabricated disk. From the top-view SEM image [Fig. 1(a)], the disk shape has negligible deformation from a circle, and the disk radius is 9.2 μm. The high-magnification tilt-view SEM image [Fig. 1(c)] reveals the roughness of the disk sidewall. As will be discussed later, such disorder is crucial to the realization of lasing-mode control that is otherwise impossible for a perfectly smooth disk.

The lasing experiment was conducted on an individual microdisk mounted in a low-temperature cryostat. The experimental setup was similar to the one described in Ref. [19]. The InAs quantum dots (QDs) were optically excited by a mode-locked Ti:sapphire laser ($\lambda_p = 790$ nm, 76 MHz, 200 fs pulses). As shown schematically in Fig. 1(d), the spatial intensity distribution of the pump beam was modulated by a spatial light modulator (Hamamatsu X10468-02), and then projected onto the top surface of a microdisk by a long-working distance objective lens. The emitted light was scattered out of the disk plane at the disk edge; some of it was collected by the same objective lens and focused into a multimode fiber which was connected to a spectrometer. Since the high-Q modes

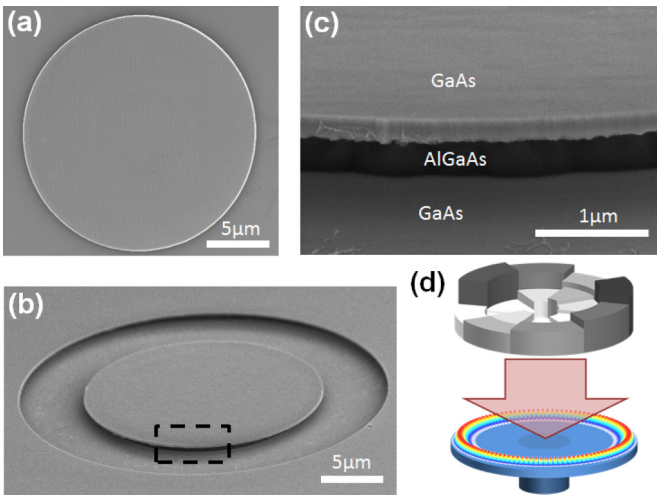

FIG. 1. (Color online) Fabricated GaAs microdisk. (a) Top-view and (b) tilt-view scanning electron microscope images of a GaAs microdisk. (c) Magnified view of the part highlighted in (b) reveals the sidewall roughness of the disk. (d) A schematic showing the spatial intensity profile of the pump beam is modulated to control the lasing modes in the microdisk.

avoid the central region of the disk where light could leak to the substrate via the pedestal, we set the pump region to a ring, as shown in the inset of Fig. 2(a). When the pump light was uniformly distributed across the ring, many modes lased simultaneously, as seen in the main panel of Fig. 2(a).

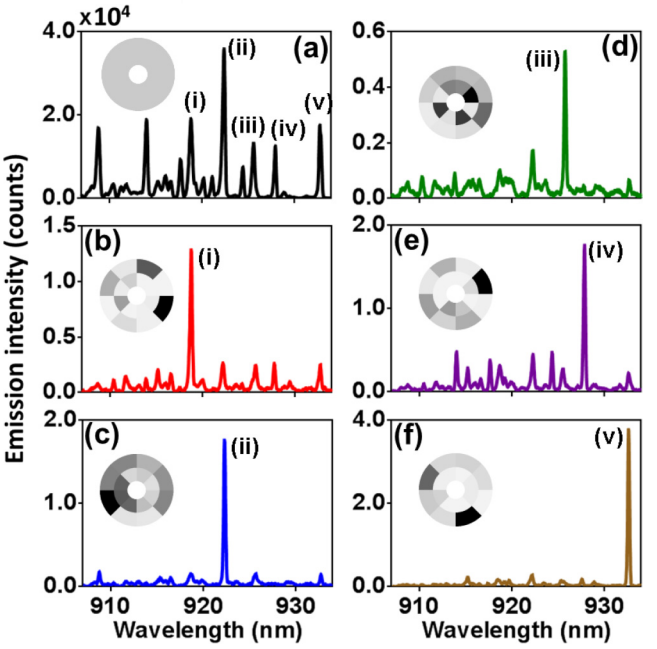

FIG. 2. (Color online) Lasing spectra with different pump patterns. (a) Under uniform ring pumping, many modes lase simultaneously. (b)–(f) Lasing spectra when modes (i)–(v) are the target as the dominant lasing mode with adaptive pumping. Insets: The final optimized pump profiles in gray scales with darker color corresponding to higher intensity.

As mentioned before, any naive attempt to select one WG mode by shaping the spatial pump profile will unavoidably enhance other WG modes with similar spatial profiles. Therefore, to make any one of the lasing modes be the dominant one, we also need to suppress all others. To achieve this, we adopt the genetic algorithm and shape the pump profile iteratively [19]. The cost function chosen for optimization is the extinction ratio $G = I_m/I_o$, where I_m is the peak intensity of the target mode and I_o is the highest intensity among all other modes. This cost function leads to optimization of the pump profile for the highest contrast between the target mode intensity and the competing mode intensities. The annular pump region on the disk is divided into two subrings; each is further divided into eight sections in the azimuthal direction. Such coarse meshing precludes any spatial selectivity of ideal WG modes in a perfectly circular disk that have the same radial number but different azimuthal number, as their azimuthal modulations of intensity differ only on a much finer length scale. The lasing modes, at least some of them, are expected to be WG modes with the lowest radial number because they have the highest-Q factor and lowest lasing threshold. Thus it would have seemed impossible to separate these modes by enhancing the spatial overlap of the pump pattern with only one of them.

Strikingly, the adaptive pumping scheme enabled any of the lasing modes to dominate over the others. Figures 2(b)–2(f) show the examples of the lasing modes labeled (i)–(v) in Fig. 2(a). Each of the panels is the lasing spectrum obtained after optimization for one of the modes, and the inset is the optimized pump profile in gray scales with darker colors representing higher intensity. The total pump power is kept at a constant value of 4 mW during the optimization process, and thus the pump power is only redistributed to a different region of the disk. After about 300 iterations of optimization, one of the modes (i)–(v) has become the dominant lasing mode with extinction ratio $G > 2.8$.

We repeated the experiment using different cost functions that either enhance the target mode intensity I_m without suppressing others or reduce the nonselected mode intensity I_o while ignoring the change of I_m. In both cases, all lasing modes are enhanced or suppressed simultaneously, without mode selection. For example, the optimization of I_m focused the pump light around the disk boundary where all of the lasing modes are concentrated. These results illustrate that the choice of an appropriate cost function is crucial to the realization of mode selection.

To understand the mechanism of mode selection, we measured the emission intensity of an individual mode as a function of the pump power for the optimized pump profile and compared to the uniform pumping. Figure 3 shows the data for the selection of mode (i). Under the uniform ring pumping, mode (i) displays a sharp increase in the growth rate of its emission intensity with the pump power P at ~3 mW, indicating the onset of lasing action. When P exceeds 4 mW, the growth rate is reduced due to gain depletion. With the optimized pump profile, mode (i) turns on at almost the same pump power, but it grows at a significantly reduced rate compared to the uniform pumping. Thus the adaptive pumping does not enhance lasing in the selected mode, instead it suppresses lasing in the nonselected modes. As an example, Fig. 3(b) plots the emission intensity of mode (iv)

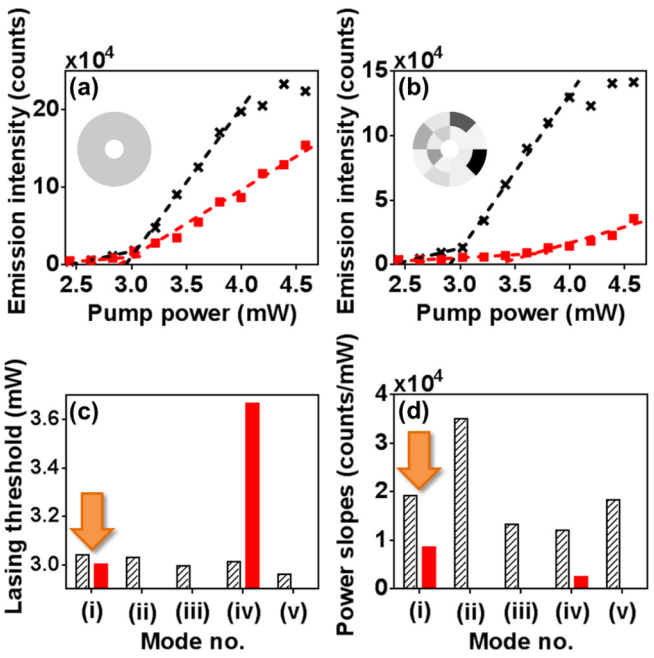

FIG. 3. (Color online) Emission intensity as a function of pump power for (a) mode (i) and (b) mode (iv) under uniform ring pumping (black crosses) and nonuniform pumping (red squares) to optimize mode (i). Insets: The intensity distribution of (a) uniform and (b) optimized pump profiles. Dashed lines represent the linear regression of the data points below and above the lasing threshold. The intersection of the two lines determines the lasing threshold pump power, and the slope of the line above the threshold gives the power slope of the lasing mode. (c),(d) Lasing thresholds and power slopes for modes (i)–(v) under uniform pumping (patterned bars) and adaptive pumping (filled bars). Mode (i) becomes the dominant lasing mode because the inhomogeneous pumping suppress all other competing modes by greatly increasing their lasing thresholds.

in the two pumping cases. Under the uniform pumping, it behaves similarly to mode (i), namely, it turns on at the pump power of 3 mW and becomes saturated beyond 4 mW. With the optimized pump profile, however, its emission is greatly reduced, as it turns on at a higher pump power of 3.65 mW and grows at a much lower rate. The other lasing modes, e.g., modes (ii), (iii), and (v), experience more suppression and do not turn on even when the pump power is increased to 5 mW.

To be more quantitative, we extract the lasing threshold and power slope of individual modes from the data. The linear fitting of the emission intensity with the pump power before and after a mode turns on gives the lasing threshold (the pump power at which the two linear lines intersect) and the power slope (the gradient of the linear fit above the threshold). The lasing thresholds and power slopes of modes (i)–(v) are plotted in Figs. 3(c) and 3(d) for uniform and selective pumping, respectively. All five modes (i)–(v) have similar lasing threshold under uniform pumping, but their power slopes exhibit more variation. After optimizing the pump profile to select mode (i), the lasing thresholds of all nonselected modes increase significantly. Even though its threshold is reduced only slightly by the adaptive pumping, the selected mode (i) has the lowest lasing threshold and

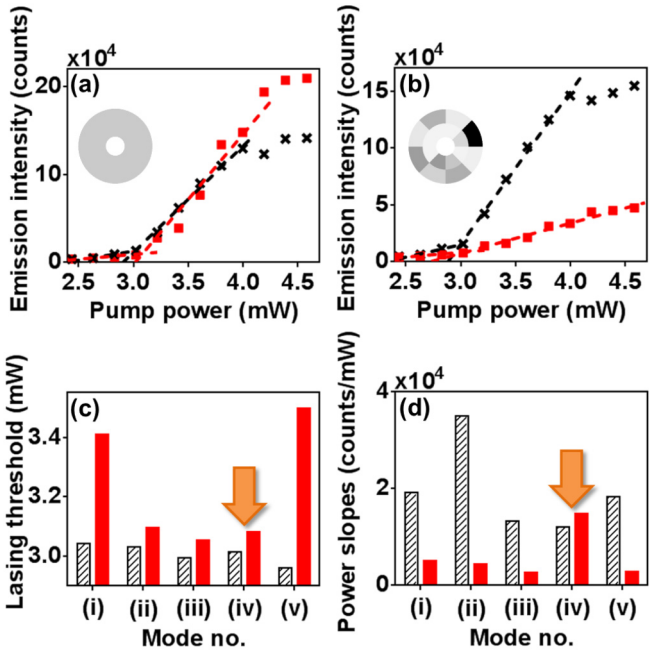

FIG. 4. (Color online) Emission intensity as a function of pump power for (a) mode (iv) and (b) mode (iii) under uniform ring pumping (black crosses) and nonuniform pumping to select mode (iv) (red squares). Insets: The intensity distribution of (a) uniform and (b) optimized pump profiles. (c),(d) Lasing thresholds and power slopes under uniform pumping (patterned bars) or selective pumping (filled bars). The target mode (iv) becomes the dominant lasing mode even though its lasing threshold is not the lowest because adaptive pumping greatly suppresses the power slopes of the competing modes.

becomes the first one to turn on. These results suggest the optimized pump profile has reduced spatial overlap with the nonselected modes, while keeping the spatial overlap with the selected mode almost the same. Given that all of the high-Q WG modes should overlap strongly at the disk boundary, the spatial discrimination achieved by the optimized pump profile is remarkable and unexpected, which will be addressed in the next section.

Increasing the difference in lasing threshold is not the only scenario to achieve mode selection; in some cases, the target mode does not have the lowest lasing threshold, but the highest power slope instead. This is seen when mode (iv) is chosen to be the dominant lasing mode (Fig. 4). With the optimized pump profile, mode (iv) is not the first one to lase, but it grows the fastest with increasing pump power above the lasing threshold, and its intensity exceeds all other modes at the pump power where the optimization is conducted. For example, mode (iii) has the lowest lasing threshold under selective pumping, so it lases first, but its power slope is much less than that with uniform pumping. In fact, the power slopes of all nonselected modes are reduced significantly by adaptive pumping and become much smaller than that of the selected mode. In contrast, the power slope of the selected mode increases slightly and the gain depletion appears at a higher emission intensity. These results suggest that the selective pumping modifies the nonlinear interaction of the lasing modes and favors the selected mode in their competition for gain.

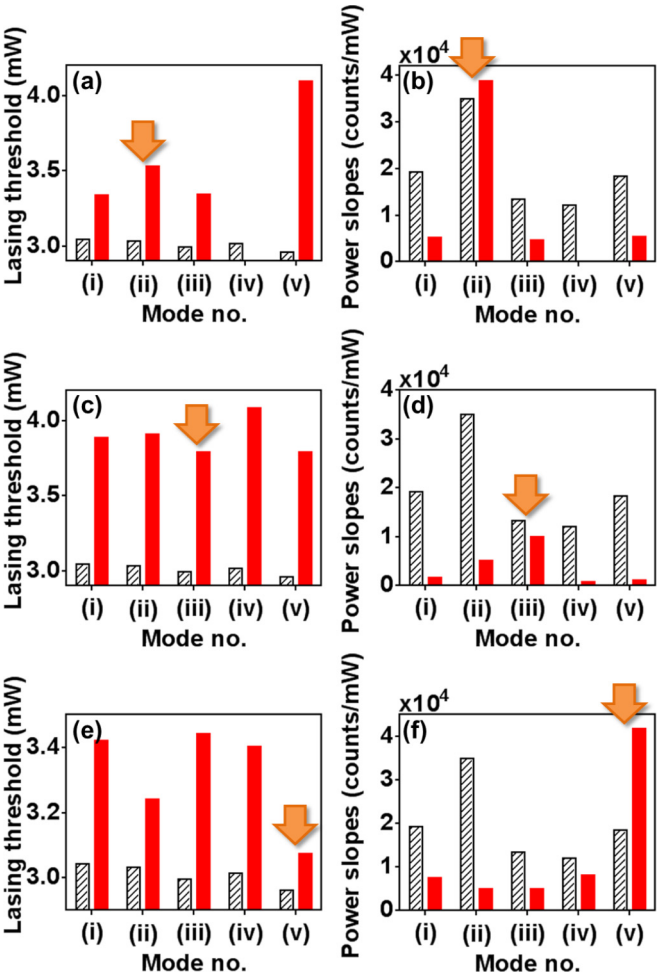

FIG. 5. (Color online) (a),(c),(e) Lasing thresholds and (b),(d),(f) power slopes for modes (i)–(v) after optimizing for modes (ii), (iii), and (v). Patterned bars represent the case for uniform pumping and filled bars are for selective pumping. While the target mode does not necessarily have the lowest lasing threshold, its power slope becomes the highest among all lasing modes.

Figure 5 shows the results for optimization of modes (ii), (iii), and (v). The selection of mode (ii) leads to a similar behavior to mode (iv): the target mode has the highest power slope instead of the lowest lasing threshold, and the power slopes of all competing modes are reduced dramatically [Figs. 5(a) and 5(b)]. In contrast, the selection of mode (iii) greatly increases the lasing thresholds of all modes including the target one and reduces their power slopes. Nevertheless, the selected mode (iii) becomes the dominant lasing mode because its power slope experiences the least reduction as compared to all other modes, especially mode (v) which has a similar lasing threshold [Figs. 5(c) and 5(d)]. To select mode (v), the lasing thresholds of all modes increase, but the increment is the smallest for the target mode and makes it the first lasing mode [Fig. 5(e)]. While the power slopes of the competing modes (i)–(iv) decrease as their thresholds increase, the power slope of mode (v) increases by a factor of two in spite of the increase of its lasing threshold. These results illustrate that the adaptive pumping is not only capable of selecting different modes to lase first by making their lasing threshold the lowest in the

linear regime (up to the first lasing threshold), but can also efficiently control the multimode lasing process in the highly nonlinear regime well above threshold.

III. THEORETICAL ANALYSIS OF LASING-MODE SELECTION

The remarkable degree of control of lasing process in the high-Q microcavity with strong mode overlap is unusual. To interpret these results, we adopt a numerical model based on the steady-state *ab initio* laser theory (SALT) [3,35,36] to compute the lasing-mode intensity under different pumping conditions. The nonlinear modal interactions included in the original form of SALT assume an homogeneously broadened gain medium, so that all of the lasing modes interact with the same population inversion and a strong lasing mode may deplete the gain available for others. The gain medium in our microdisk laser is inhomogeneously broadened, as the different sizes of InAs QDs lead to distinct emission frequencies. Since the inhomogeneous width is larger than the homogeneous width, the QDs may be grouped within each homogeneous width, and a lasing mode interacts with only one group that is in resonance with its own frequency. This seems to suggest two lasing modes with frequency spacing larger than the QD homogeneous width would interact with different groups of QDs and do not interact. However, experimentally, the pump light at $\lambda = 790$ nm generated electron-hole pairs in the GaAs layer, which subsequently relaxed to the InAs QDs. Hence, all of the QDs shared the same reservoir of carriers. When a lasing mode rapidly depleted the carriers in one group of QDs, these QDs would get replenished quickly from the GaAs layer, reducing the available carriers for other modes. Thus, the lasing modes, even with frequency spacing larger than the QD homogeneous width, competed for the carriers in the shared reservoir [37]. This competition induces nonlinear modal interactions that can be effectively captured by the SALT.

Since the high-Q modes in the GaAs microdisk have low lasing thresholds, they usually lase and their frequencies and spatial profile are barely changed by the pump. Thus, each lasing mode can be approximated by a single quasibound mode in the passive cavity [35]; and the interactions of lasing modes, through the gain medium, only affect their lasing thresholds and intensities above threshold. This "single-pole" approximation (SPA) simplifies the SALT formula to the following set of equations [36]:

$$\frac{D_0}{D_0^{(\mu)}} - 1 = \sum_{\nu} \Gamma_\nu \chi_{\mu\nu} I_\nu, \tag{1}$$

which are linear in terms of the pump strength D_0 and the lasing-mode intensities I_μ. $D_0^{(\mu)}$ is the threshold of mode μ for a given pump profile $f(\vec{r})$ and in the absence of modal interactions. If $f(\vec{r})$ is normalized by $\int_p f(\vec{r})d\vec{r} = A$, where the subscript "$p$" denotes integration over the ring-shaped pump region of area A, $D_0^{(\mu)}$ is simply given by [7]

$$D_0^{(\mu)} \approx \frac{n^2}{Q_\mu \mathrm{Re}[f_\mu]}, \quad f_\mu \equiv \int_c f(\vec{r})\Psi_\mu^2(\vec{r})d\vec{r}, \tag{2}$$

where the subscript "c" denotes integration over the entire microdisk. Here, n is the refractive index of the microdisk, and Q_μ and $\Psi_\mu(\vec{r})$ are the Q factor and wave function of mode μ, respectively. $\Psi_\mu(\vec{r})$ is normalized using $\int_c \Psi_\mu^2(\vec{r})d\vec{r} = 1$. As evident in Eq. (2), the direct outcome of n on-uniform pumping is modifying the noninteracting threshold $D_0^{(\mu)}$ through the pump overlapping factor f_μ. In general f_μ is a complex number, but for the high-Q modes in the microdisk, it is approximately a real number. For uniform pumping across the ring, $f(\vec{r})$ is equal to 1 inside the ring and 0 outside the ring. Thus, $f_\mu = 1$, since the high-Q WG modes have little overlap with the central region of the disk that is on top of the pedestal. Γ_ν on the right-hand side of Eq. (1) is the Lorentzian gain factor of the lasing mode ν, which can be taken as 1 because each lasing mode interacts only with the resonant QDs, as mentioned above. The interaction matrix χ contains the self-interaction coefficients ($\mu = \nu$) and cross-interaction coefficients ($\mu \neq \nu$) of the lasing modes. Because the lasing modes in the microdisk cavity correspond to the high-Q modes, χ can be defined as

$$\chi_{\mu\nu} = \frac{1}{A}\left|\int_c d\vec{r}\ \Psi_\mu^2(\vec{r})\,|\Psi_\nu(\vec{r})|^2\right|. \tag{3}$$

Note that the interaction matrix itself does not change with the pump profile $f(\vec{r})$; the effect of the latter is reflected by the changes in the lasing threshold and power slope above threshold.

Excellent agreement has been obtained between the results of the SPA-SALT equations (1) and the direct numerical solution to the Maxwell-Bloch equations in previous studies [36,38]. The latter approach is extremely demanding in terms of computational power and time, which is impractical for our analysis here. We note that the SALT incorporates the modal interactions to infinite order, which is preserved in the SPA. To illustrate how the SPA-SALT captures the modification of gain saturation by selective pumping, let us consider the simplest case of single-mode lasing. The power slope of the lasing mode (mode 1), defined by dI_1/dD_0, can be found from Eqs. (1) and (2), $S_1 = [\chi_{11}D_0^{(1)}]^{-1} = Q_1\mathrm{Re}[f_1]/\chi_{11}n^2$. Its value is proportional to the pump overlapping factor and inversely proportional to the self-interaction coefficient. Thus, changing the pump profile will modify the power slope of the lasing mode via nonlinear self-saturation of gain.

In the discussion below, we will show that the mechanisms of different mode selection scenarios observed experimentally can be illustrated with the interactions of two modes only, and we will focus on the role of nonuniform pumping. The lasing threshold and power slope of the second lasing mode strongly depend on its interaction with the first lasing mode. Because of this interaction, the threshold of the second mode is not $D_0^{(2)}$, but rather

$$D_{0,\mathrm{int}}^{(2)} = \frac{\chi_{11}/\chi_{21} - 1}{\chi_{11}/\chi_{21} - D_0^{(2)}/D_0^{(1)}} D_0^{(2)}. \tag{4}$$

We will refer to $D_{0,\mathrm{int}}^{(\mu)}$ as the interacting threshold and $D_0^{(\mu)}$ as the noninteracting threshold. For the first lasing threshold, $D_{0,\mathrm{int}}^{(1)} = D_0^{(1)}$. The second lasing mode has a higher noninteracting threshold, $D_0^{(2)} > D_0^{(1)}$, and its interacting threshold

$D^{(2)}_{0,\mathrm{int}}$ is further increased by the interaction between modes 1 and 2, $D^{(2)}_{0,\mathrm{int}} > D^{(2)}_0$. The power slope of the second lasing mode is given by

$$S_{2,\mathrm{int}} = \frac{\chi_{11}/\chi_{21} - D^{(2)}_0/D^{(1)}_0}{\chi_{11}/\chi_{21} - \chi_{12}/\chi_{22}} S_2, \tag{5}$$

where $S_2 = [\chi_{22} D^{(2)}_0]^{-1} = Q_2 \mathrm{Re}[f_2]/\chi_{22} n^2$ is its power slope in the absence of interaction with mode 1. Due to the modal interaction, the power slope of the first lasing mode is changed to

$$S_{1,\mathrm{int}} = \frac{\chi_{22}/\chi_{12} - D^{(1)}_0/D^{(2)}_0}{\chi_{22}/\chi_{12} - \chi_{21}/\chi_{11}} S_1, \tag{6}$$

once the second mode starts lasing.

To see how the nonlinear modal interaction can be controlled by selective pumping, let us consider two pump profiles, $f(\vec{r})$ and $\tilde{f}(\vec{r})$.

According to the above equations, different pump profiles will change both the lasing threshold and power slope of the second lasing mode through the noninteracting threshold $D^{(\mu)}_0$. The resulting changes of both quantities reflect the nonlinear effects induced by the modification of pump profile. If there were no nonlinear interaction between modes 1 and 2, by modifying the pump profile from a particular $f(\vec{r})$ to another one $\tilde{f}(\vec{r})$, the lasing threshold of the second mode would change from $D^{(2)}_0 = n^2/Q_2 f_2$ to $\tilde{D}^{(2)}_0 = n^2/Q_2 \tilde{f}_2$, with $\tilde{f}_2$ defined by having $\tilde{f}(\vec{r})$ in Eq. (2). However, the actual threshold of mode 2 is given by Eq. (4) instead, with $D^{(\mu)}_0$ replaced by the corresponding $\tilde{D}^{(\mu)}_0$, and its dependence on the noninteracting threshold of the first lasing mode reflects the modal interaction that varies with the pump profile. Similarly, the power slopes of both modes, given by Eqs. (5) and (6), depend on the ratio of $D^{(1)}_0$ and $D^{(2)}_0$, indicating that both self-saturation and cross-saturation effects can be modified by the pump profile.

To quantify the change of the nonlinear effects due to the variation of the pump profile, we use the ratio of the power slopes $\tilde{S}_{2,\mathrm{int}}$ [with pump profile $\tilde{f}(\vec{r})$] and $S_{2,\mathrm{int}}$ [with pump profile $f(\vec{r})$] for mode 2:

$$\mathcal{M}_2 \equiv \frac{\tilde{S}_{2,\mathrm{int}}}{S_{2,\mathrm{int}}} = \frac{\tilde{f}_2 \chi_{11}/\chi_{21} - Q_1 \tilde{f}_1/Q_2}{f_2 \chi_{11}/\chi_{21} - Q_1 f_1/Q_2}. \tag{7}$$

We note that this modification factor $\mathcal{M}_2$ also governs the change of the interacting threshold of mode 2, i.e., $D^{(2)}_{0,\mathrm{int}}/\tilde{D}^{(2)}_{0,\mathrm{int}} = \mathcal{M}_2$. For mode 1, the ratio of its power slopes after mode 2 lases is

$$\mathcal{M}_1 \equiv \frac{\tilde{S}_{1,\mathrm{int}}}{S_{1,\mathrm{int}}} = \frac{\tilde{f}_1 \chi_{22}/\chi_{12} - Q_2 \tilde{f}_2/Q_1}{f_1 \chi_{22}/\chi_{12} - Q_2 f_2/Q_1}. \tag{8}$$

Therefore, we see that besides the pump overlapping factors and the Q factors, two important modal interaction parameters are the ratios of the interaction coefficients: χ_{11}/χ_{21} and χ_{22}/χ_{12}.

Next we will apply the above formula to the analysis of lasing-mode selection by adaptive pumping. If mode 1 is the dominant lasing mode with uniform pumping, there are two scenarios to make mode 2 dominant by nonuniform pumping. The first one is to have mode 2 lase first by lowering its noninteracting threshold to below that of mode 1, similar to the scenario shown in Fig. 3. Since $D^{(\mu)}_0$ scales inversely with the pump overlapping factor, nonuniform pumping may enhance the pump overlap with mode 2 and/or reduce the pump overlap with mode 1. This requires little spatial overlap between mode 1 and 2, which is not true for the high-Q WG modes in a perfect circular microdisk. However, the disk sidewall roughness, albeit small, has a profound effect on the mode profiles, as we will illustrate with numerical simulation.

Due to the finite resolution of the scanning electron microscope (SEM), we could not map the exact boundary roughness to compute the lasing modes observed experimentally. Also, a disk of radius $\sim$10 μm supports many high-Q modes, and the experimental uncertainty about the disk temperature during optical pumping leads to an inaccurate estimation of the refractive index, making the matching of lasing frequencies between simulation and experiment extremely difficult. As a compromise, we chose to simulate a smaller disk with radius 3 μm to provide a physical understanding of the effects of adaptive pumping. The effective index of refraction of the disk is set to $n = 3.13$ [39]. We introduced surface roughness on the disk boundary by adding random high-order harmonic perturbations; the disk boundary is described in the polar coordinates as $\rho(\theta) = R + \sum_{m=20}^{80} a_m \cos(m\theta + \phi_m)$, where a_m and ϕ_m are random numbers in the range $[-0.5$ nm, 0.5 nm] and $[-\pi, \pi]$, respectively. The highest-order harmonic perturbation, $m = 80$, is chosen to be slightly larger than $2\pi n R/\lambda$ because light in the cavity cannot resolve boundary modulation much finer than its wavelength λ/n. The lowest-order harmonic perturbation, $m = 20$, limits the scale of boundary modulation to be less than 1 μm, which is consistent with the SEM images of the fabricated microdisks.

We calculated the quasibound modes of the passive cavity using the finite-element frequency-domain method [40]. Two of the high-Q modes with transverse electric (TE) polarization (electric field parallel to the disk plane) are shown in Figs. 6(a) and 6(b). Their Q factors are $Q_1 \simeq 1.20 \times 10^5$ and $Q_2 \simeq 1.09 \times 10^5$, respectively. They are both WG modes, but exhibit additional features than the regular WG modes. In mode 1 [Fig. 6(a)], the counterclockwise (CCW) propagating WG wave dominates over the clockwise (CW) wave, reducing the contrast between the field intensity maxima and minima. By expanding the intracavity field distribution in the cylindrical harmonics, we identify that its radial number is 1 and azimuthal number is 57. Similar analysis of mode 2 [Fig. 6(b)] reveals that in addition to the primary WG wave with radial number 1 and azimuthal number 58, it has additional WG waves of higher radial order number 7 and azimuthal number 34. This is attributed to the mixing of WG modes with different order via wave scattering by the rough boundary of the microdisk [32–34].

Using these mode profiles, we find that the interaction parameters are $\chi_{11}/\chi_{21} = 1.64$ and $\chi_{22}/\chi_{12} = 1.44$. Under uniform ring pumping, $f_1 = f_2 = 1$, and $D^{(2)}_0/D^{(1)}_0 = Q_1/Q_2 = 1.1$. Mode 1 lases first due to its higher Q factor, as illustrated in Fig. 6(c), where the pump strength D_0 is normalized to the first lasing threshold $D^{(1)}_0$. We numerically simulated adaptive pumping using the same polar grid as in experiment (i.e., double rings, each divided further into eight regions of equal

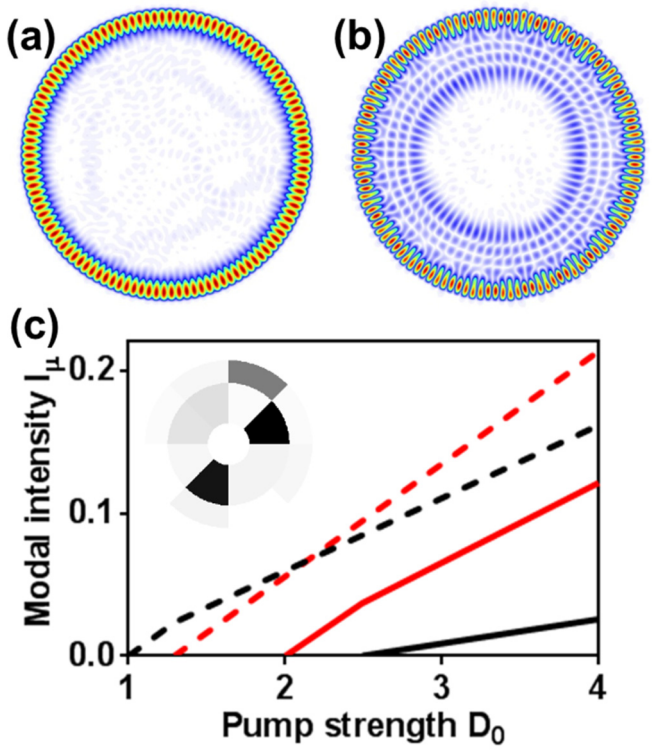

FIG. 6. (Color online) Numerical simulation of switching of lasing order by adaptive pumping of a microdisk with rough boundary. The disk radius is 3 μm and the refractive index is 3.13. (a),(b) Calculated spatial distribution of magnetic field ($|H_z|$) for two TE-polarized high-Q modes, labeled mode 1 and 2, respectively. Mode 1, at $\lambda = 917.7$ nm, has Q factor of 1.20×10^5. Mode 2, at $\lambda = 902.9$ nm, has Q factor of 1.09×10^5. Mode 1 in (a) consists predominantly of CCW propagating WG wave with radial number 1 and azimuthal number 57. Mode 2 in (b) is primarily a WG modes of radial number 1 and azimuthal number 58, but contains additional WG waves of higher radial order number 7 due to disorder-induced mode mixing. (c) Lasing intensity for modes 1 and 2 as a function of pump strength D_0 with uniform ring pumping (dashed lines) or nonuniform pumping to select mode 2 (solid lines). Mode 1 lases first before mode 2 with uniform pumping, but the lasing order switches, i.e., mode 2 lases first, with the nonuniform pump profile (inset) shown in the gray scale with darker color corresponding to stronger pumping. D_0 is normalized to the lasing threshold of mode 1 with uniform ring pumping.

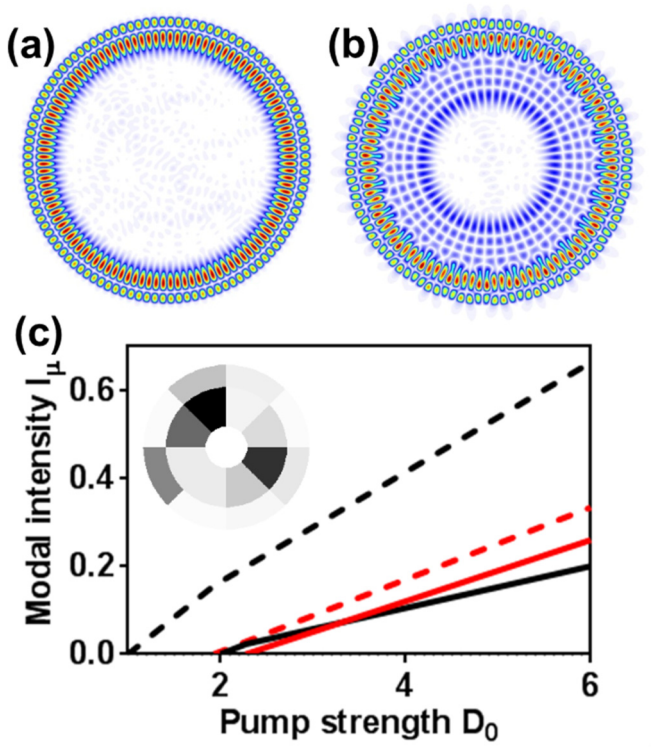

FIG. 7. (Color online) Numerical simulation of changing the power slopes of lasing modes by adaptive pumping of a microdisk with rough boundary. The disk radius is 3 μm and the refractive index is 3.13. (a),(b) Calculated spatial distribution of magnetic field ($|H_z|$) for two WG modes of second radial order, labeled mode 1 and 2, respectively. (c) Lasing intensity for these two modes with uniform ring pumping (dashed lines) and nonuniform pumping to make mode 2 stronger than mode 1 (solid lines). The optimized pump profile found by the genetic algorithm does not change the lasing order but greatly suppresses the power slope of mode 1 (black lines).

area). For each pump pattern, we first calculated the pump overlapping factor and the noninteracting threshold for the two modes, then solved Eq. (1) to find the modal intensities. To enhance lasing in mode 2, we ran the genetic algorithm to maximize the intensity ratio of mode 2 over mode 1, I_2/I_1, by redistributing the pump energy across the ring while keeping the total pump strength fixed at $D_0 = 3$. The adaptive pumping switches the order of lasing, as shown in Fig. 6(c), and mode 2 lases first. The pump overlapping factor for mode 1 is reduced to $\tilde{f}_1 = 0.47$, and mode 2 to $\tilde{f}_2 = 0.55$. Both modes have higher lasing thresholds due to reduced spatial overlap with the pump. Nevertheless, the optimized pump pattern has larger overlap with mode 2 by shifting most pump energy to the inner ring. This is only possible because mode 2 extends more into the inner ring by disorder-induced mixing of different WG modes. The larger pump overlapping factor of mode 2 overcomes its lower-Q factor, $\tilde{f}_2/\tilde{f}_1 > Q_1/Q_2$, making $D_0^{(2)} < D_0^{(1)}$.

The second scenario of making the second lasing mode stronger than the first is to modify their power slopes without switching the order of lasing. This is similar to the scenario observed in Fig. 4, and the selectivity was enabled by the strong suppression of the power slopes of all other lasing modes, including the one with the lowest threshold (mode 1 here). In Figs. 7(a) and 7(b), we consider another pair of high-Q modes with TE polarization, and their Q factors are $Q_1 \simeq 1.31 \times 10^5$ and $Q_2 \simeq 1.05 \times 10^5$, respectively. By decomposing their intracavity field distributions by cylindrical harmonics, we confirm that both modes consist primarily of second radial order WG modes. In addition, mode 2 contains additional field components from another nearby low-Q WG mode of a higher radial order due to disorder-induced mode mixing. Using their mode profiles, we find that the interaction parameters are $\chi_{11}/\chi_{21} = 1.71$ and $\chi_{22}/\chi_{12} = 1.43$.

Under uniform ring pumping ($f_1 = f_2 = 1$), $D_0^{(2)}/D_0^{(1)}$ is given by $Q_1/Q_2 = 1.25$, and mode 1 turns on first due to its higher Q factor. Its power slope is higher than that of mode 2,

as shown in Fig. 7(c), with the pump strength D_0 normalized by $D_0^{(1)}$. After the optimization process to maximize I_2/I_1 at $D_0 = 3$, the pump overlap factors are changed to $\tilde{f}_1 = 0.5$ and $\tilde{f}_2 = 0.59$. Even though the optimized pump profile has a stronger overlap with mode 2 by concentrating pump energy to the inner ring [inset of Fig. 7(c)], the change is not sufficient to compensate the difference in the Q factor, i.e., $\tilde{f}_2/\tilde{f}_1 < Q_1/Q_2$, and mode 1 remains the first lasing mode as $\tilde{D}_0^{(1)} < \tilde{D}_0^{(2)}$. Nevertheless, the power slope of mode 2, calculated with Eq. (5), is reduced only by $1 - \mathcal{M}_2 = 17\%$ according to Eq. (7). In contrast, the power slope of mode 1 is reduced by $1 - \mathcal{M}_1 = 61\%$, which is much more than mode 2. Consequently, the power slope of mode 2 becomes higher than mode 1 with nonuniform pumping, and thus its lasing intensity exceeds that of mode 1 at $D_0 > 3.3$. This result shows that adaptive pumping can enhance lasing in the target mode through nonlinear modal competition above threshold and modify the power slopes of lasing modes significantly. Such capability could not be achieved by the conventional pump engineering of semiconductor microcavity lasers [20–31].

IV. DISCUSSION AND CONCLUSION

For a smooth microdisk without boundary roughness, we have verified numerically that adaptive pumping does not work for the corresponding WG modes in the previous examples or any other high-Q WG modes with same radial order. These modes have very similar spatial profiles which cannot be differentiated by the coarse modulation of the pump region, and hence preclude any spatial selectivity. For example, the genetic algorithm could not find an optimized pump profile that switches the lasing order of the two WG modes (without disorder) in Fig. 6 because the ratio of their pump overlapping factors $\tilde{f}_2/\tilde{f}_1$ remains the same for different pump patterns. Compared to a smooth microdisk, the disorder on the disk boundary results in the generation of diversified mode profiles with different pump overlapping factors and interaction coefficients, as confirmed in our numerical simulation. Such diversity is expected to scale up with the disk size, as the density of high-Q WG modes increases, and the reduced frequency spacing facilitates the mixing of WG modes with different radial order. Thus, the larger disks used in our experiment have more versatile interactions among the lasing modes, which can be controlled by shaping the spatial pump profile.

Compared to the weakly scattering random lasers which have a large spatial degree of freedom, the high-Q microcavity lasers inherently have less degree of control. Nevertheless, we demonstrate that the intrinsic fabrication imperfection enables the diversified modal interactions that can be utilized to control the lasing behavior. We believe our method can be extended to electrical pumping by patterning the contact electrodes and controlling the current injection, creating a tunable on-chip light source for integrated photonic applications.

ACKNOWLEDGMENTS

We thank Patrick Sebbah, Nicolas Bachelard, Stefan Rotter, Douglas Stone, Alex Cerjan, and Jan Wiersig for stimulating discussion. This work is supported by the Office of Naval Research under Grant No. ONR MURI SP0001135605 and by the National Science Foundation under Grant No. DMR-1205307.

[1] T. Harayama, P. Davis, and K. S. Ikeda, Stable oscillations of a spatially chaotic wave function in a microstadium laser, Phys. Rev. Lett. **90**, 063901 (2003).

[2] L. Angelani, C. Conti, G. Ruocco, and F. Zamponi, Glassy behavior of light, Phys. Rev. Lett. **96**, 065702 (2006).

[3] H. E. Türeci, L. Ge, S. Rotter, and A. D. Stone, Strong interactions in multimode random lasers, Science **320**, 643 (2008).

[4] N. Bachelard, J. Andreasen, S. Gigan, and P. Sebbah, Taming random lasers through active spatial control of the pump, Phys. Rev. Lett. **109**, 033903 (2012).

[5] M. Leonetti, C. Conti, and C. Lopez, Switching and amplification in disordered lasing resonators, Nat. Commun. **4**, 1740 (2013).

[6] N. Bachelard, S. Gigan, X. Noblin, and P. Sebbah, Adaptive pumping for spectral control of random lasers, Nat. Phys. **10**, 426 (2014).

[7] L. Ge, O. Malik, and H. E. Türeci, Enhancement of laser power-efficiency by control of spatial hole burning interactions, Nat. Photon. **8**, 871 (2014).

[8] M. Liertzer, L. Ge, A. Cerjan, A. D. Stone, H. E. Türeci, and S. Rotter, Pump-induced exceptional points in lasers above threshold, Phys. Rev. Lett. **108**, 173901 (2012).

[9] M. Brandstetter, M. Liertzer, C. Deutsch, P. Klang, J. Schöberl, H. E. Türeci, G. Strasser, K. Unterrainer, and S. Rotter, Reversing the pump dependence of a laser at an exceptional point, Nat. Commun. **5**, 4034 (2014).

[10] B. Peng, S. K. Özdemir, S. Rotter, H. Yilmaz, M. Liertzer, F. Monifi, C. M. Bender, F. Nori, and L. Yang, Loss-induced suppression and revival of lasing, Science **346**, 328 (2014).

[11] R. El-Ganainy, M. Khajavikhan, and L. Ge, Exceptional points and lasing self-termination in photonic molecules, Phys. Rev. A **90**, 013802 (2014).

[12] L. Ge and A. D. Stone, Parity-time symmetry breaking beyond One dimension: The role of degeneracy, Phys. Rev. X **4**, 031011 (2014).

[13] L. Feng, Z. J. Wong, R.-M. Ma, Y. Wang, and X. Zhang, Single-mode laser by parity-time symmetry breaking, Science **346**, 972 (2014).

[14] H. Hodaei, M. Miri, M. Heinrich, D. N. Christodoulides, and M. Khajavikhan, Parity-time-symmetric microring lasers, Science **346**, 975 (2014).

[15] M. Leonetti, C. Conti, and C. Lopez, The mode-locking transition of random lasers, Nat. Photon. **5**, 615 (2011).

[16] M. Leonetti and C. López, Active subnanometer spectral control of a random laser, Appl. Phys. Lett. **102**, 071105 (2013).

[17] *Optical Processes in Microcavities*, edited by R. K. Chang and A. J. Campillo, Advanced Series in Applied Physics (World Scientific, Singapore, 1996).

[18] *Optical Microcavities*, edited by K. J. Vahala, Advanced Series in Applied Physics (World Scientific, Singapore, 2004).

[19] S. F. Liew, B. Redding, L. Ge, G. S. Solomon, and H. Cao, Active control of emission directionality of semiconductor microdisk lasers, Appl. Phys. Lett. **104**, 231108 (2014).

[20] S. F. Pereira, M. B. Willemsen, M. P. van Exter, and J. P. Woerdman, Pinning of daisy modes in optically pumped vertical-cavity curface-emitting lasers, Appl. Phys. Lett. **73**, 2239 (1998).

[21] N. B. Rex, R. K. Chang, and L. J. Guido, Threshold lowering in GaN micropillar lasers by means of spatially selective optical pumping, IEEE Photon. Technol. Lett. **13**, 1 (2001).

[22] Y. F. Chen, Y. P. Lan, and S. C. Wang, Generation of Laguerre Gaussian modes in fiber-coupled laser diode end-pumped lasers, Appl. Phys. B **72**, 167 (2001).

[23] Y. F. Chen and Y. P. Lan, Laguerre-Gaussian modes in a double-end-pumped microchip laser: Superposition and competition, J. Opt. B **3**, 146 (2001).

[24] T. Fukushima, T. Harayama, P. Davis, P. O. Vaccaro, T. Nishimura, and T. Aida, Ring and axis mode lasing in quasi-stadium laser diodes with concentric end mirrors, Opt. Lett. **27**, 1430 (2002).

[25] G. D. Chern, H. E. Tureci, A. D. Stone, R. K. Chang, M. Kneissl, and N. M. Johnson, Unidirectional lasing from InGaN multiple-quantum-well spiral-shaped micropillars, Appl. Phys. Lett. **83**, 1710 (2003).

[26] J.-F. Bisson, A. Shirakawa, Y. Sato, Y. Senatsky, and K.-I. Ueda, Near-field diffractive optical pumping of a laser medium, Opt. Rev. **11**, 353 (2004).

[27] M. Kneissl, M. Teepe, N. Miyashita, N. M. Johnson, G. D. Chern, and R. K. Chang, Current-injection spiral-shaped microcavity disk laser diodes with unidirectional emission, Appl. Phys. Lett. **84**, 2485 (2004).

[28] M. Hentschel, T.-Y. Kwon, M. A. Belkin, R. Audet, and F. Capasso, Angular emission characteristics of quantum cascade spiral microlasers, Opt. Express **17**, 10335 (2009).

[29] M. Hentschel and T.-Y. Kwon, Designing and understanding directional emission from spiral microlasers, Opt. Lett. **34**, 163 (2009).

[30] S. Shinohara, T. Harayama, T. Fukushima, M. Hentschel, T. Sasaki, and E. E. Narimanov, Chaos-assisted directional light emission from microcavity lasers, Phys. Rev. Lett. **104**, 163902 (2010).

[31] D. Naidoo, T. Godin, M. Fromager, E. Cagniot, N. Passilly, A. Forbes, and K. Aït-Ameur, Transverse mode selection in a monolithic microchip laser, Opt. Commun. **284**, 5475 (2011).

[32] L. Ge, Q. Song, B. Redding, and H. Cao, Extreme output sensitivity to subwavelength boundary deformation in microcavities, Phys. Rev. A **87**, 023833 (2013).

[33] L. Ge, Q. Song, B. Redding, A. Eberspächer, J. Wiersig, and H. Cao, Controlling multimode coupling by boundary-wave scattering, Phys. Rev. A **88**, 043801 (2013).

[34] B. Redding, L. Ge, Q. Song, G. S. Solomon, and H. Cao, Manipulation of high-order scattering processes in ultrasmall optical resonators to control far-field emission, Phys. Rev. Lett. **112**, 163902 (2014).

[35] H. E. Türeci, A. D. Stone, and B. Collier, Self-consistent multimode lasing theory for complex or random lasing media, Phys. Rev. A **74**, 043822 (2006).

[36] L. Ge, Y. D. Chong, and A. D. Stone, Steady-state *ab initio* laser theory: Generalizations and analytic results, Phys. Rev. A **82**, 063824 (2010).

[37] S. Strauf, K. Hennessy, M. T. Rakher, Y.-S. Choi, A. Badolato, L. C. Andreani, E. L. Hu, P. M. Petroff, and D. Bouwmeester, Self-tuned quantum dot gain in photonic crystal lasers, Phys. Rev. Lett. **96**, 127404 (2006).

[38] A. Cerjan, Y. D. Chong, L. Ge, and A. D. Stone, Steady-state *ab initio* laser theory for *n*-level lasers, Opt. Express **20**, 474 (2012).

[39] Q. H. Song, L. Ge, J. Wiersig, J.-B. Shim, J. Unterhinninghofen, A. Eberspächer, W. Fang, G. S. Solomon, and H. Cao, Wavelength-scale deformed microdisk lasers, Phys. Rev. A **84**, 063843 (2011).

[40] www.comsol.com.